Chemical Intercalation of Topological Insulator Grid Nanostructures for High-Performance Transparent Electrodes

Yunfan Guo, Jinyuan Zhou, Yujing Liu, Xu Zhou, Fengrui Yao, Congwei Tan, Jinxiong Wu, Li Lin, Kaihui Liu, Zhongfan Liu, and Hailin Peng*

2D layered nanomaterials with strong covalent bonding within layers and weak van der Waals' interactions between layers have attracted tremendous interest in recent years. Layered Bi_2Se_3 is a representative topological insulator material in this family, which holds promise for exploration of the fundamental physics and practical applications such as transparent electrode. Here, a simultaneous enhancement of optical transmittance and electrical conductivity in Bi_2Se_3 grid electrodes by copper-atom intercalation is presented. These Cu-intercalated 2D Bi_2Se_3 electrodes exhibit high uniformity over large area and excellent stabilities to environmental perturbations, such as UV light, thermal fluctuation, and mechanical distortion. Remarkably, by intercalating a high density of copper atoms, the electrical and optical performance of Bi_2Se_3 grid electrodes is greatly improved from 900 Ω sq^{-1}, 68% to 300 Ω sq^{-1}, 82% in the visible range; with better performance of 300 Ω sq^{-1}, 91% achieved in the near-infrared region. These unique properties of Cu-intercalated topological insulator grid nanostructures may boost their potential applications in high-performance optoelectronics, especially for infrared optoelectronic devices.

Besides graphene,[1–3] 2D-layered materials such as topological insulators Bi_2X_3 (X = Se, Te)[4–6] and a variety of transition-metal dichalcogenides[7] have hosted extensive attention in a diverse fields of nanoelectronics,[8] thermoelectrics,[9] energy storage technologies,[10] and flexible optoelectronics,[11] due to their intriguing properties and 2D-layered structures.

Dr. Y. Guo, Dr. Y. Liu, C. Tan, Dr. J. Wu, Dr. L. Lin, Prof. Z. Liu, Prof. H. Peng
Center for Nanochemistry
Beijing Science and Engineering Center for Nanocarbons
Beijing National Laboratory for Molecular Sciences
College of Chemistry and Molecular Engineering
Peking University
Beijing 100871, P. R. China
E-mail: hlpeng@pku.edu.cn
Dr. J. Zhou, X. Zhou
Academy for Advanced Interdisciplinary Studies
Peking University
Beijing 100871, P. R. China
F. Yao, Prof. K. Liu
State Key Laboratory for Mesoscopic Physics
School of Physics
Center for Nanochemistry
Peking University
Beijing 100871, P. R. China

Strikingly, the large interlayer separation in layered materials provides the ideal space to accommodate guest species through intercalation,[12–22] a process that has been widely used for exfoliation of few-layer nanomaterials,[13,14] as a new strategy for energy storage,[15,16] converting the physical nature of topological insulators,[17–19] and introducing new ternary or quaternary layered nanomaterials with preeminent properties.[20–22] Particularly, it has been reported that the electronic structures of host materials can be tuned controllably by intercalation treatment,[23] which can give rise to higher optical transmittance and better electrical conductivity simultaneously.[24–26] These properties are highly desired for transparent electrodes, an indispensable component in efficient optoelectronics.[27]

Topological insulators (TI),[28–30] with insulating bulk gap and metallic Dirac surface states, have motivated tremendous research interests in the past decade. Owing to their topologically protected and spin-momentum-locked Dirac surface states, few-layer topological insulator nanostructures are predicted to be competitive material for broadband optoelectronic devices, such as terahertz lasers, infrared photodetectors, and transparent electrodes.[31] In our previous works, we reported the first experimental demonstration of near-infrared transparent electrodes based on few-layer Bi_2Se_3 nanosheets[32] by van der Waals' epitaxy. Compared with indium tin oxide (ITO), the prototype material in the field of transparent electrode, topological electrodes exhibits good conductivity, broad and high transmittance, as well as excellent mechanical flexibility and chemical durability.[32] Regarding the transparency and conductivity of TI electrodes, further improvements have been achieved by gridding Bi_2Se_3 films[33] and hybridizing Dirac materials between Bi_2Se_3 and graphene.[34] Despite these achievements, more efforts need to be devoted for better electrode performances. For example, increased transmittance of Bi_2Se_3 grids in the visible range was realized at the cost of lower electrical conductivity with reduced material consumption.[33] Therefore, it is essential and challenging to improve the transmittance and conductivity simultaneously for topological electrodes.

To tackle the above issue, herein, we explored a facile chemical method to intercalate high density of zero-valent

ADVANCED
SCIENCE NEWS
www.advancedsciencenews.com

ADVANCED
MATERIALS
www.advmat.de

copper atom in topological insulator Bi_2Se_3 grid electrodes. Large-area Cu-intercalated Bi_2Se_3 grids with well-defined locations and tailored configurations are produced by selective-area van der Waals' epitaxy similar to our earlier works.[35,36] Up to 37 at% copper atoms were intercalated into Bi_2Se_3 through a low-temperature disproportionation redox reaction.[37–39] In contrast with pristine Bi_2Se_3 grids, Cu-intercalated Bi_2Se_3 grid electrodes demonstrate an obviously improved optical transmittance in a wide range of wavelength, for the fact that large amounts of free electrons were injected into the host structure, elevating the Fermi level (E_F) into the conduction band significantly. As a result, the effective bandgap is enlarged and normal interband transition is blocked. In terms of electrical conductivity, due to the ultrahigh carrier density introduced by copper intercalation, the sheet resistance (R_s) decreased dramatically by one to threefold, realizing the co-instantaneous improvement in transparency and conductivity. Surprisingly, the typical performance of Cu-intercalated Bi_2Se_3 grid electrodes can be raised from 68%, 900 Ω sq^{-1} to 82%, 300 Ω sq^{-1} at 550 nm, and better performance around 91%, 300 Ω sq^{-1} can be achieved in the near infrared region. In addition, since these copper dopants are accommodated between the adjacent layers of Bi_2Se_3, which would be protected from various external perturbations, the Cu-intercalated Bi_2Se_3 grid electrodes exhibit outstanding mechanical stability and chemical durability for practical applications.

Bi_2Se_3, a typical layered topological insulator, possesses a rhombohedral crystal structure in space group D_{3d}^5 (R-$3m$). Each planar layer consists of five covalently bonded atoms ordered in Se–Bi–Se–Bi–Se sequence along c-axis, stacking together by van der Waals' interaction. The large van der Waals' gap ($\approx$2.57 Å) in Bi_2Se_3 supplies perfect location to accommodate copper atoms as shown in **Scheme 1**a. Scheme 1b illustrates the flexible transparent electrode made by Cu-intercalated Bi_2Se_3 grids.

In order to compare the changes introduced by intercalation, systematic characterizations have been performed for Bi_2Se_3 grid nanostructures. Optical microscopy images in transmission mode were taken for the same Bi_2Se_3 grids before and after intercalation on a large scale. Sharp color contrasts in **Figure 1**a,b and Figure S1 (Supporting Information) demonstrate that Bi_2Se_3 grids look much more transparent after 40 min Cu intercalation under the same illumination condition. Atomic force microscopy (AFM) was used to determine the thickness variation and surface morphology of Bi_2Se_3 grid electrodes in Figure 1c,d and Figure S2 (Supporting Information). The AFM image and height profile of a $\approx$28 nm thick Bi_2Se_3 strip reveal a flat surface with terraced structures.[40] After intercalation, the thickness of the identical flake increases from 28.3 to 39.2 nm due to volume expansion (Figure 1d), which has also been found in Li$^+$ intercalated MoS_2 films.[41] It was reported that the height increase of Bi_2Se_3 is not only attributed to the insertion of Cu atoms in interlayer gaps, but also caused by lattice expansion along the a and c axes of the Bi_2Se_3 crystal.[37] Possibly, the lattice expansion would make a difference on the interlayer interaction of Bi_2Se_3, which could be probed by low-wavenumber Raman spectral measurements. Figure 1e describes four representative Raman modes of Bi_2Se_3 crystal, including two A_{1g} modes ($\approx$72 and $\approx$174 cm^{-1}) and two E_g modes ($\approx$37 and $\approx$131 cm^{-1}). The A_{1g} modes correspond
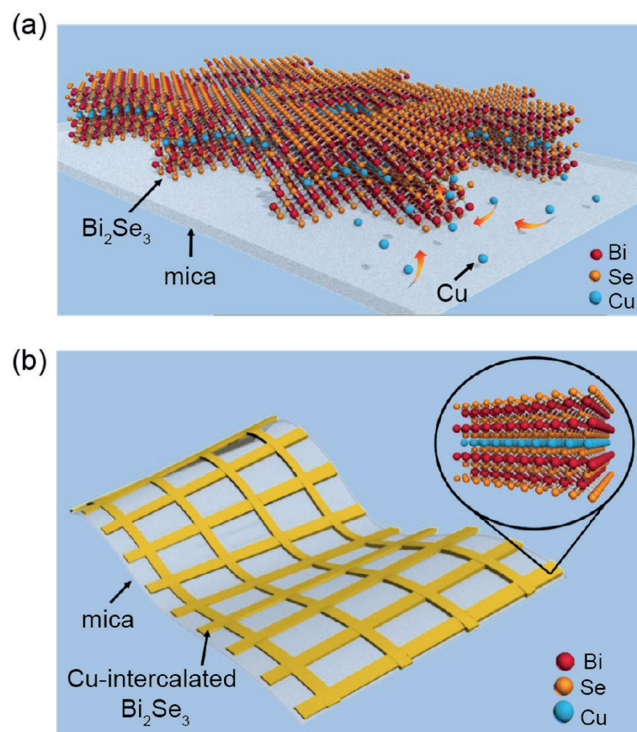
Scheme 1. a) Schematic diagram of copper intercalation process in Bi_2Se_3 grid nanostructures. b) Schematic diagram of flexible transparent electrode made by Cu-intercalated Bi_2Se_3 nanogrids.

to the out of plane modes parallel to the c-axis, while the E_g modes account for in-plane bonding vibrations perpendicular to c-axis.[42] We focused on the individual Bi_2Se_3 grid sample before and after intercalation (Figure 1f), and made the corresponding Raman characterization. As shown in Figure 1g, the Raman signals for pristine Bi_2Se_3 grids correspond well with A_{1g}^1, E_g^2, and A_{1g}^2 modes as in literature.[43] Under the same reaction time (10 min), no noticeable shift was detected for A_{1g} modes after intercalation in 1×10^{-3}, 10×10^{-3}, and 20×10^{-3} M tetrakis(acetonitrile)copper(I) hexafluorophosphate solutions, respectively. This indicates that no bonding interaction exists between Cu atom and the host material. Otherwise, there would be obvious Raman shift or broadening as a result of phonon softening.[39] On the other hand, the in-plane E_g modes change evidently. The E_g^2 peak becomes broader in higher concentration, which may originate from the increase of structure defects or impurity scattering by volume expansion. Notably, the E_g^1 mode, sensitive to interlayer interaction, grows up in higher concentrations, which would be related to the stronger phonon–electron force after intercalation.

To evaluate the structure and quality of Cu-intercalated Bi_2Se_3 grids, we carried out transmission electron microscopy (TEM) study. Free-standing Bi_2Se_3 grids were fully transferred from mica substrate onto a Mo TEM grid with the assistance of a poly(methyl methacrylate)-mediated method[44,45] (**Figure 2**a). Different from traditional intercalation, this solution-based chemical interaction approach would not induce cation exchange or disrupt the host lattice. From the close-up view in Figure 2b, the surface morphology of Bi_2Se_3 grid after Cu intercalation is still intact and flat. This is in stark contrast with

ADVANCED
SCIENCE NEWS
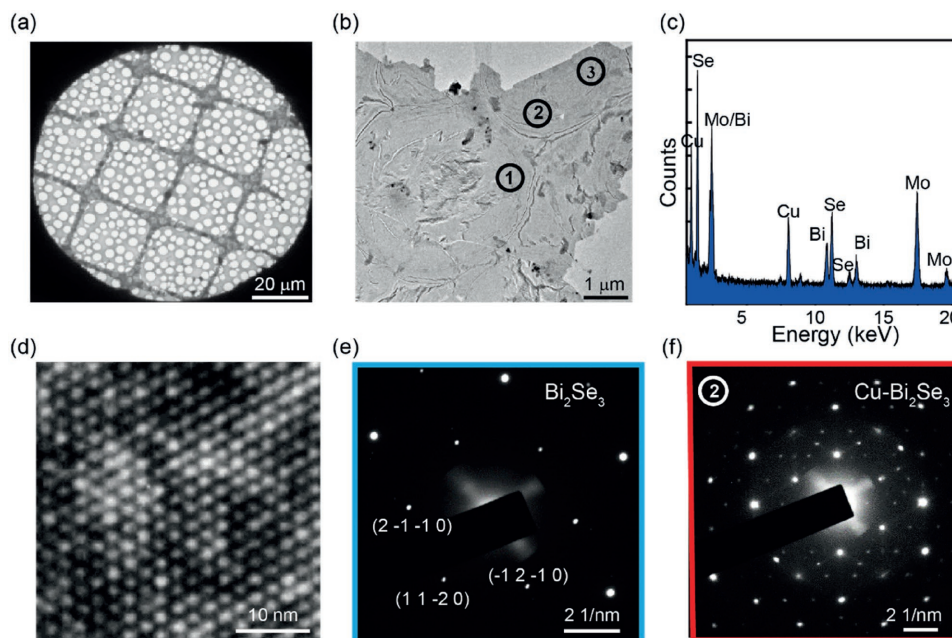www.advancedsciencenews.com

ADVANCED
MATERIALS
www.advmat.de
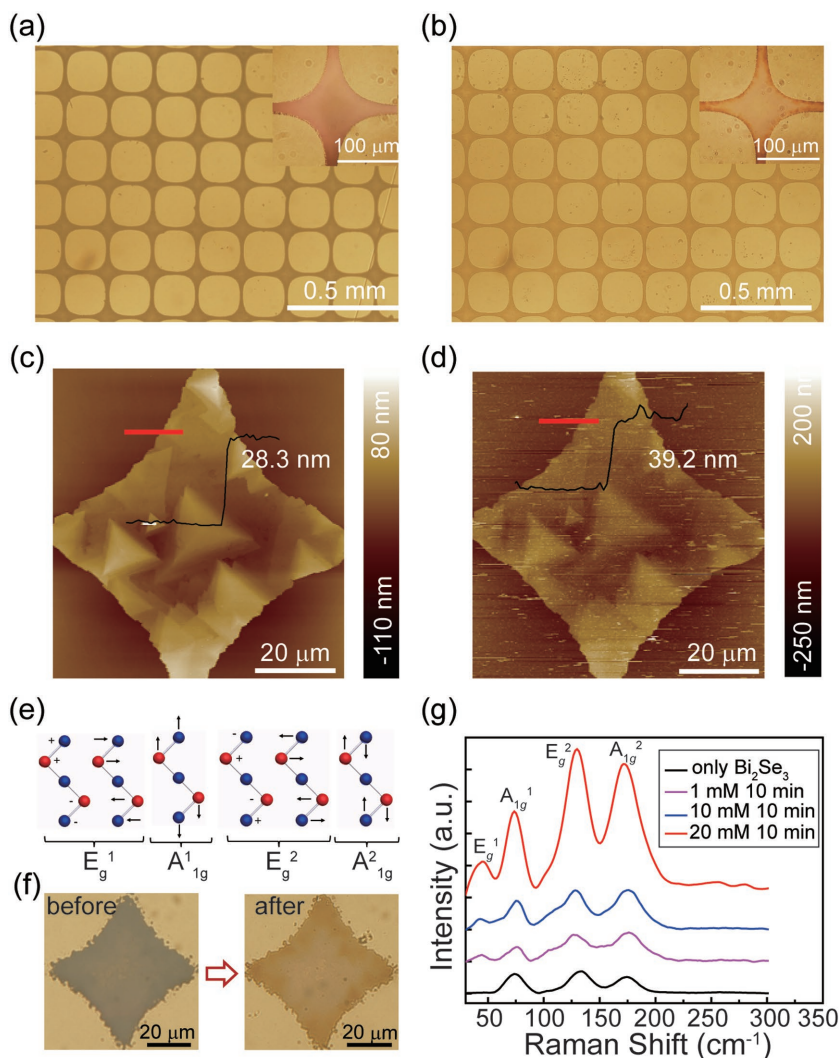
Figure 1. a,b) Typical optical microscopy images in transmission mode of large-area, few-layer Bi_2Se_3 grids before and after Cu intercalation on mica substrate. c,d) AFM images and the height profiles of an individual Bi_2Se_3 grid before and after Cu intercalation. e) The typical Raman active vibrational modes of Bi_2Se_3. f) Optical images of one individual Bi_2Se_3 grid before and after Cu-intercalation for Raman measurement. g) Low-wavenumber Raman scattering spectra for Cu-intercalated Bi_2Se_3 grids with different intercalating concentrations.

In addition to high crystalline quality, Cu-intercalated Bi_2Se_3 grids exhibit significant improvements in optical performance from the visible to the near infrared region. First, we studied the variations in optical transmission for individual Bi_2Se_3 grid by microspot transmission measurement. As shown in **Figure 3**a, the light spot diameter is only around 2 μm, much smaller than the lateral size of Bi_2Se_3 grid. Figure 3b and Figure S4a (Supporting Information) exhibit the microspot transmission spectrum of ≈30 nm-thick Bi_2Se_3 grids before (black) and after (red) intercalation for 40 and 20 min, respectively. At the wavelength of 550 nm, we observed that the optical microspot transmittance of the Bi_2Se_3 grid increased rapidly from 15% to 58% after intercalation (Figure 3b). In Figure 3c, the microspot transmittance difference (ΔT) grows from 10% to 50% for Bi_2Se_3 grids with similar thickness, when the reaction time increased from 10 to 40 min. On the other hand, the evaluation for optical performance is indispensable on a macroscopic scale. As shown in Figure 3d, the transmittance of Bi_2Se_3 grid in aperture size of 150 μm is improved from 81% (black line) to 90% (red) in the visible range, and better performance from 85% to 97% in the near infrared region. Figure S4b (Supporting Information) shows the transmittance change of Bi_2Se_3 grid in aperture size of 70 μm. In Figure 3e, the transmittance change of Bi_2Se_3 grids before and after intercalation is displayed at wavelength of 550 nm with different thicknesses. Note that all grid samples show a drastic increase in transparency. For example, the transmittance of pristine Bi_2Se_3 grid of 25 nm thick rises up from 74% to 90%. Higher transmittance up to 94% is achieved by thinner grids with 20 nm in thickness. Additionally, the optical performance can also be controlled by changing solvent concentrations. Figure 3f illustrates that higher concentration (≈20 × 10⁻³ M) promotes better transmittance for Bi_2Se_3 grid electrodes. Qualitatively, the transmission enhancement can mainly be attributed to the substantial electron doping from intercalation on ultrathin nanogrids. Similar to the situation in metal intercalated graphene,[47,48] the large amount of free electrons introduced by Cu intercalation effectively elevated the Fermi level (E_F) of Bi_2Se_3 into the conduction band,[24] which shows an obvious n-doping effect and results in suppressed interband optical transition (the inset of Figure 3f).
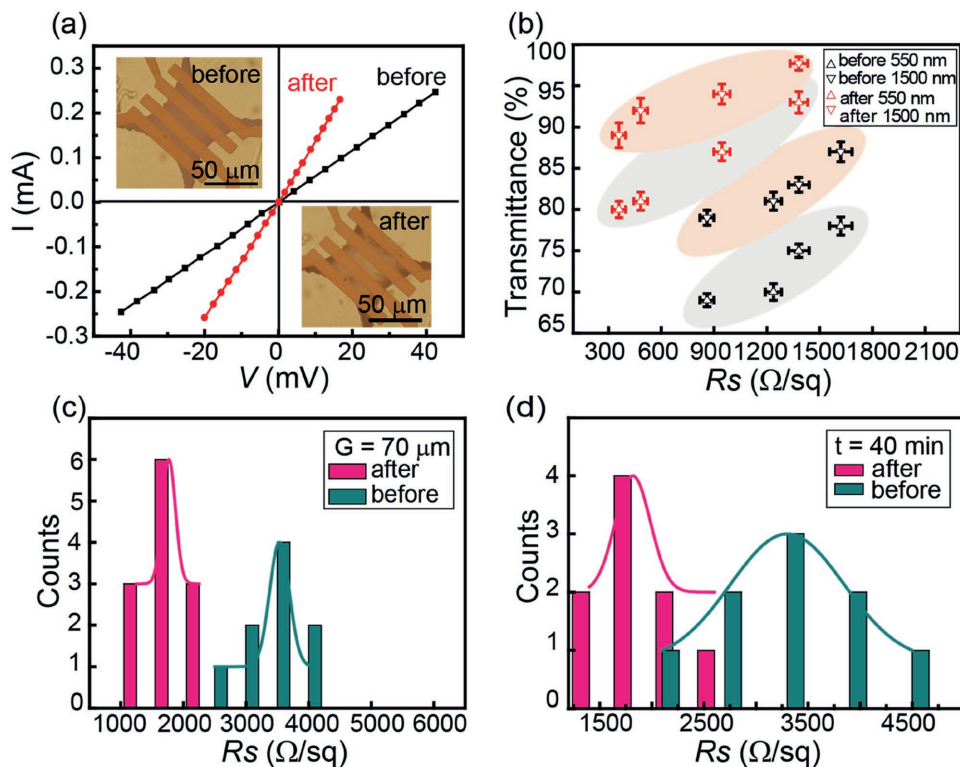
Together with the increasing optical transmittance, Bi_2Se_3 grid electrodes also exhibit improved electrical conductivity due to ultrahigh carrier density by Cu intercalation. Standard 4-probe measurement was conducted on individual Bi_2Se_3 grid device in **Figure 4**a. It is shown that the Bi_2Se_3 channel becomes more transparent and the chromium/gold

the controlled sample intercalated by Cu^{2+},[38] which exhibits a large amount of voids due to the cation exchange with Bi^{2+}. Furthermore, another convincing proof from energy dispersive X-ray (EDX) spectrum shows that the ratio of Bi:Se remains 2:3, even when the atomic ratio of copper reaches as high as 37% (Figure 2c). The high-resolution TEM (HRTEM) image in Figure 2d shows that Cu-intercalated Bi_2Se_3 grid maintains high crystal quality. Remarkably, the observation of superlattice structure with electron diffraction is a sign of intercalation. For the pristine Bi_2Se_3 grid (Figure 2e), selected area electron diffraction (SAED) displays regular hexagonal patterns without any additional diffraction spots. After intercalation, with enough copper atoms entering the host lattice, the copper atoms occupied ordered sites and form striking superlattice spots in SAED patterns (Figure 2f and Figure S3, Supporting Information), which was observed in Na-intercalated TiS_2 as well.[46]

Figure 2. a) Bright-field TEM image of a free standing Cu-intercalated Bi_2Se_3 grid transferred from a mica substrate. b) Low-resolution TEM image of a Cu-intercalated Bi_2Se_3 grid. c) EDX spectrum of a Bi_2Se_3 grid with a high percentage of Cu intercalation. d) HRTEM image of the Cu-intercalated grid in (b), showing the highly crystalline nature. e) SAED patterns of the pristine Bi_2Se_3 grid. f) Representative superlattice SAED patterns observed with copper intercalation, indicating the interlayer ordering of Cu atom within Bi_2Se_3 host.
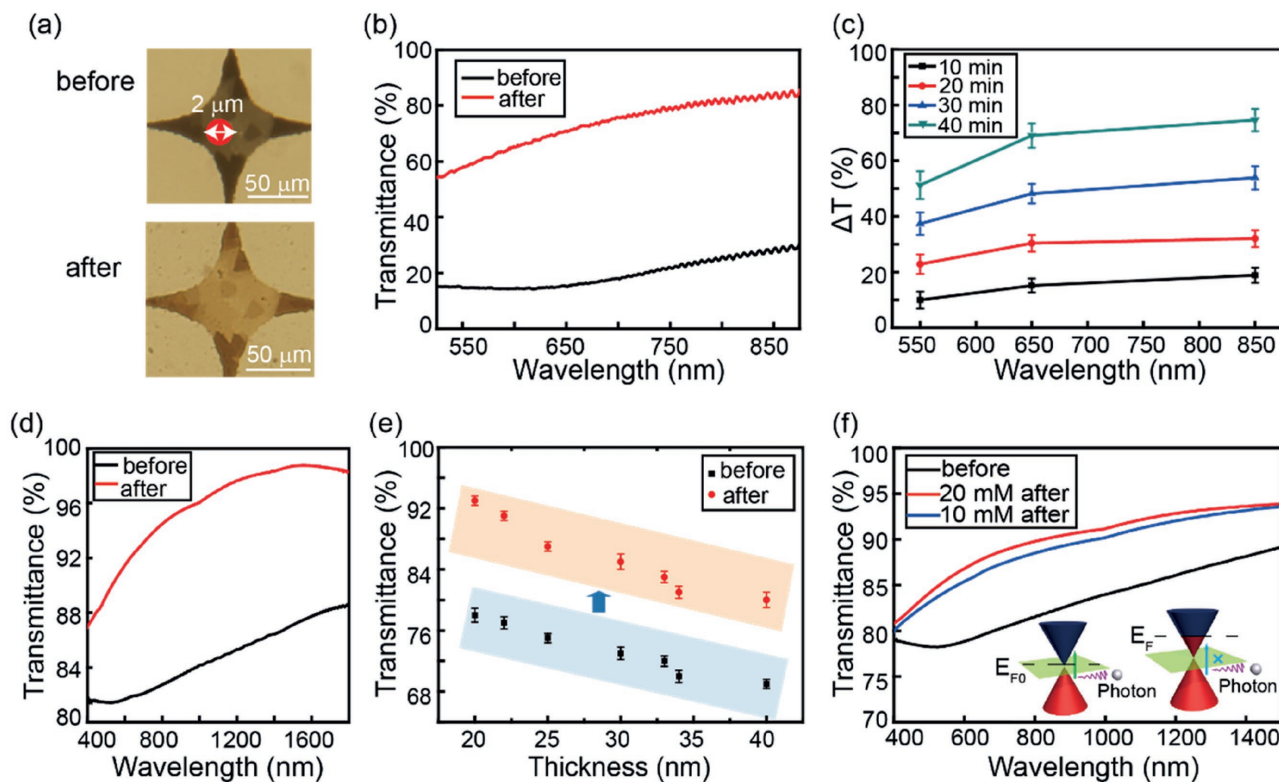
Figure 3. Optical characterization of Bi_2Se_3 grid electrodes. a) Optical microscopy images in transmission mode of a 30 nm thick Bi_2Se_3 gird on mica substrate before and after Cu intercalation. b) Microoptical–transmission spectrum of Bi_2Se_3 grid before (black) and after (red) 40 min Cu intercalation. c) Intercalation time dependence of transmittance difference (ΔT) between before and after reaction for Bi_2Se_3 grids at the wavelength of 550, 650, and 850 nm, respectively. d) Optical transmission spectrum for a 30 nm thick Bi_2Se_3 grid with aperture size of 150 µm before (black) and after (red) Cu intercalation. e) The growth of optical transmission at the wavelength of 550 nm for Bi_2Se_3 grids with different thickness. f) Optical transmission spectrum for pristine Bi_2Se_3 grids (black) and grids intercalated with the concentrations of 10×10^{-3} M (blue) and 20×10^{-3} M (red), respectively.

**ADVANCED
SCIENCE NEWS**

www.advancedsciencenews.com

**ADVANCED
MATERIALS**

www.advmat.de

Figure 4. Electrical characterization of Bi_2Se_3 grid electrodes. a) Source–drain current (I) versus voltage (V) characteristics for Bi_2Se_3 grid before and after intercalation. Upper left inset: optical image of a 4-probe device based on pristine Bi_2Se_3 grid; lower right inset: optical image of a 4-probe device based on Cu-intercalated Bi_2Se_3 grid. b) Transmission-R_s map shows the synergistic enhancement in both transparency and conductivity for Cu-intercalated Bi_2Se_3 grids. c) Histogram of sheet resistance distribution of a 40 min Cu-intercalated Bi_2Se_3 grids with aperture size of 70 µm. d) Histogram of sheet resistance distribution of a 100 µm aperture size Cu-intercalated Bi_2Se_3 grids intercalated for 40 min.

(5 nm/50 nm) contact remains intact after intercalation (insets of Figure 4a). Both current–voltage (I–V) curves keep linear and symmetric, indicating the good contact between Bi_2Se_3 grid and metal electrodes. Remarkably, the sheet resistance (R_s) of Bi_2Se_3 grids reduced dramatically by one to threefold when copper atoms were inserted into Bi_2Se_3 host. For instance, the R_s of a 35 nm thick grid decreased from 1300 to 420 Ω sq^{-1} (Figure S5, Supporting Information). In terms of transparent electrode, higher optical transparency and lower electrical resistance are particularly desired. To further evaluate the performance of Cu-intercalated Bi_2Se_3 grid electrode, we illustrate a map between R_s and transmittance at the wavelength of 550 and 1500 nm (Figure 4b). In the visible range, the performance of Bi_2Se_3 grids improved from 68%, 900 Ω sq^{-1} to 82%, 300 Ω sq^{-1} with copper intercalants, showing a simultaneous enhancement in optical transmittance and electrical conductivity, which is comparable with the performance of roll-to-roll graphene and carbon nanotube transparent electrode[49] (Figure S6, Supporting Information). Moreover, higher value of 91%, 300 Ω sq^{-1} can be achieved in the near-infrared region, which is much better than the performance of pristine Bi_2Se_3 grid electrode.[32] On the other hand, the evaluation for electrical conductivity on a large scale should not be ignored. We used photolithography to fabricate electrode arrays. For Bi_2Se_3 grids with different aperture sizes, the R_s distribution histograms show that, the average R_s for grids with aperture size of 70, 100, and 150 µm decreased from 3500, 4100,

and 6000 Ω sq^{-1} to 1500, 2000, and 2800 Ω sq^{-1}, respectively (Figure 4c and Figure S7a,b, Supporting Information). In addition, it is convenient to adjust the conductivity by changing reaction time of intercalation. The histograms in Figure 4d and Figure S7c,d (Supporting Information) show that the average R_s for Bi_2Se_3 grids decreased from 4400, 4100, and 3300 Ω sq^{-1} to 2500, 2100, and 1700 Ω sq^{-1} when intercalated for 20, 30, and 40 min, respectively. Therefore, benefiting from the ultrahigh electron density by copper intercalation, the optical transparency enhancement together with the large increase in conductivity creates promising opportunities for Bi_2Se_3 grids as high-performance transparent electrodes.

Besides high transmittance and conductivity, transparent electrodes also call for outstanding chemical durability in practical applications. According to the previous studies,[27] a variety of factors such as chemical agents, UV light illumination, and elevated temperature might cause degradation in performance of traditional transparent electrode materials. In terms of carbon-based transparent electrode, strong oxidants like $SOCl_2$[50] and $TCNQF_4$[51] are often used to achieve substantial doping level for higher conductivity. However, these adsorptive dopants are innately unstable under UV illumination or high temperatures, which would give rise to unrecoverable degradation for host materials. In our case, the exotic copper dopants are sealed up in a limited space between adjacent quintuple layers (QLs) of Bi_2Se_3 crystal, as illustrated in **Figure 5**a, which may protect them from various environmental perturbations.
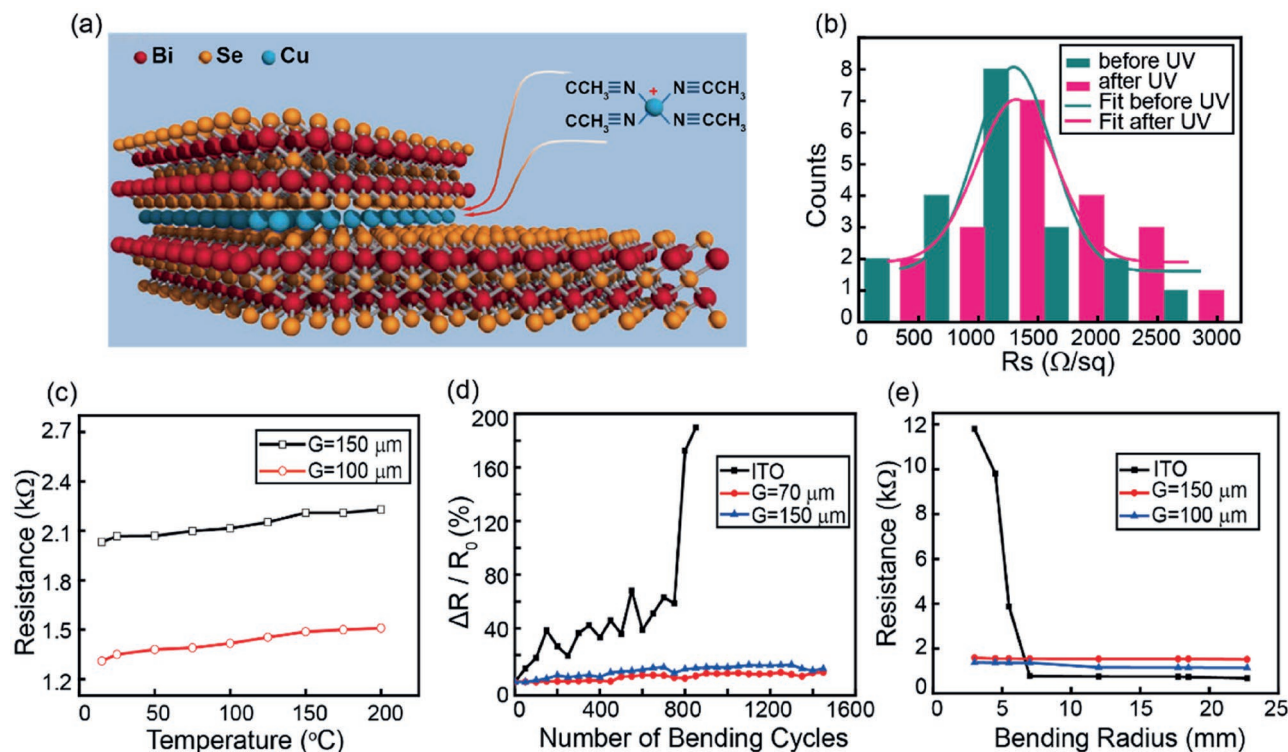
Figure 5. Chemical and mechanical stability of Cu-intercalated Bi_2Se_3 grid electrodes. a) Schematic diagram for the high stability of Cu-intercalated Bi_2Se_3 grid. b) Histogram of sheet resistance distribution for ≈40 nm thick Cu-intercalated Bi_2Se_3 grids before and after 30 s UV light treatment. c) Temperature dependence of electrical resistance for Cu-intercalated Bi_2Se_3 grids with aperture sizes of 100 and 150 μm. d) Resistance change with respect to bending cycles for a Cu-intercalated Bi_2Se_3 grid electrodes with aperture sizes of 70 and 150 μm, and the nearly thick ITO film. e) Resistance change of ITO film and Cu-intercalated Bi_2Se_3 grid electrodes (100 and 150 μm) for different bending radius.

In order to evaluate the stability of Cu-intercalated Bi_2Se_3 grid electrode, we compared its resistance variation before and after designed treatments. First, we exposed Bi_2Se_3 grids under UV light for 30 s. The histogram in Figure 5b shows that the average R_s of Bi_2Se_3 grids slightly changes from 1270 to 1400 Ω sq^{-1}, indicating great stability under UV illumination. Furthermore, during the thermal treatment, the intercalated Bi_2Se_3 grids remained intact and kept good conductivity after being heated to 200 °C (Figure 5c). Different from conventional doping method, the accommodation of copper atoms between the QLs of Bi_2Se_3 grid electrodes guarantees outstanding chemical stabilities for practical applications.

Mechanical flexibility is another indispensable element for transparent electrodes in the next generation of flexible optoelectronics. The predominant material ITO is relatively brittle, which limits its wide application in flexible optoelectronic devices. In contrast, Cu-intercalated Bi_2Se_3 nanogrids display significant flexibility together with attractive optical transmittance and conductivity (Figure S8, Supporting Information). Figure 5d compares the conductance change in the ratio of ΔR ($= R - R_0$) to R_0 for ITO and Cu-intercalated Bi_2Se_3 grids with two aperture sizes (70 and 150 μm). For ITO, the $\Delta R/R_0$ gradually increased to 75% in the first 580 bending cycles. After 780 cycles, it rises up to 100%, implying the failure of ITO device. In sharp contrast, the $\Delta R/R_0$ for Cu-intercalated Bi_2Se_3 grid electrodes are always below 8% over 1500 cycles of bending, verifying its good flexibility. In addition, we also performed a

test on the conductivity of ITO and Bi_2Se_3 grid electrodes with different bending radius. As shown in Figure 5e, compared with the dramatic decrease in the resistance of ITO, there is unnoticeable change in the conductivity of Cu-intercalated Bi_2Se_3 electrodes when the bending radius decreased down to 3 mm. In all, since this gentle chemical intercalation does not disturb the 2D planar structure of layered Bi_2Se_3, mechanical durability is successfully inherited from pristine Bi_2Se_3 grids after intercalation. Combined with the topologically protected surface states, which remain conductive under a high density of dislocations or defects, Cu intercalated-Bi_2Se_3 grid electrodes exhibit great potential for dissipationless interconnects and flexible transparent electrodes.

In summary, we successfully intercalated high density of zero-valent copper atoms into 2D layered Bi_2Se_3 grid nanostructure by utilizing a gentle chemical intercalation method. The well-defined intercalated Bi_2Se_3 grids show promise as efficient flexible transparent electrodes, presumably because the ultrahigh carrier density introduced by intercalation could lead to the simultaneous enhancement in optical transmittance and electrical conductivity from the visible range to the near-infrared region. In addition, the Cu-intercalated Bi_2Se_3 grid electrodes possess outstanding chemical stability and mechanical flexibility, for the fact that the copper atoms accommodated in van der Waals' gaps are protected from external perturbations. These remarkable properties of Cu-intercalated Bi_2Se_3 grid electrodes may inspire exciting prospects for its

application in novel flexible optoelectronics, especially for infrared nanoelectronics.

Experimental Section

Synthesis of Bi₂Se₃ Grid Nanostructures: Bi_2Se_3 grid nanostructures were grown on prepatterned fluorophlogopite mica substrate by physical vapor deposition inside a 12 in. horizontal tube furnace with a 1 in. diameter quartz tube. The raw material Bi_2Se_3 power (Alfa Aesar, purity 99.999%) was placed in the center of the tube furnace (460–500 °C) for evaporation. Prepatterned mica substrates were placed downstream at certain locations in the tube. Ultrapure argon was used as carrier gas to transport hot Bi_2Se_3 vapor to cold mica. After the tube was pumped to a low pressure about 10 mTorr and flushed with the carrier gas repeatedly to remove air contamination, the growth of Bi_2Se_3 grid nanostructures started. Typical growth conditions were a pressure of 50 Torr, source temperature of 490 °C, growth time of 10–40 min, gas flow rate of 200 sccm (standard cubic centimeters per minute), and growth temperature below 280–390 °C.

Intercalation of Bi₂Se₃ Grid Nanostructures: Copper atoms were intercalated into Bi_2Se_3 host in a disproportionation redox reaction.[31–33] Before intercalation, all glassware was cleaned with distilled water and dried in a hot oven. Bi_2Se_3 grid nanostructures on mica substrates were laid under reflux (≈52 °C) in a solution of (1–20) × 10⁻³ M of tetrakis(acetonitrile)copper(I) hexafluorophosphate (Sigma-Aldrich) in acetone for 10–40 min. The initial pH of the solution was 5.0–6.5. Then, the copper intercalated Bi_2Se_3 grids were removed from solution, rinsed with hot acetone and ethanol (45 °C) repeatedly, and finally dried with pure nitrogen gas.

Characterization: Characterization was conducted by using optical microscopy (Olympus DX5r1 microscope) and AFM (Vecco Nanoscope IIIa); TEM images, SEAD, and energy dispersive X-ray analysis were measured with TEM (FEI Tecnai F30; acceleration voltage, 300 kV). Optical transmission was characterized by UV–vis–IR (Perkin Elmer Lambda 950 spectrophotometer). Microspot transmission data were collected by a home-built confocal microscope system, where a supercontinuum laser (420–2300 nm) was used as the light source, the objective (Mitutoyo M Plan 80×, N.A. = 0.5) served to focus the supercontinuum light to the sample and then objective (Mitutoyo M Plan 50×, N.A. = 0.65) collected the light. Two sets of spectra with the sample inside beam (T_{sample}) and outside beam ($T_{substrate}$) were taken by a hydrogen liquid camera (Princeton Instruments PYL100BRX) and the final microspot transmission spectrum $\Delta T/T = (T_{sample} - T_{substrate})/T_{substrate}$ was obtained. Low-wavenumber Raman scattering measurements were collected by a home-built confocal micro-Raman microscopy system Princeton Instruments Acton SP 2500i). The Raman scattering spectra were excited by a $\lambda = 532$ nm solid state laser. The spectra resolution was ≈1 cm⁻¹, the focused spot size was ≈1 µm, and the lowest available frequency was ≈10 cm⁻¹ by a set of 532 nm BragGrate Notch Filter (532 BNF). Electrical measurements were carried out in a Micromanipulator 6200 probe station with a Keithley 4200 semiconductor analyzer.

Device Fabrication: Dielectric mica substrate was compatible with standard device fabrication procedures, which facilitated the transfer-free of 4-probe devices. Standard EBL (STRATA DB 235, FEI) and photolithography were carried out for the 4-probe array devices fabrication. Plasma etching (50 W, 30 Pa) and thermal evaporation (UNIVEX 300, Leybold Vacuum) were used to separate certain regions for target device structure and deposited chromium/gold (5 nm/50 nm) as metal electrodes. At last, the device was lifted-off by hot acetone and blow dried with nitrogen gas.

Transport Measurement: A semiconductor analyzer (Keithley, SCS-4200) was used to measure the four terminal electrical properties.

Supporting Information

Supporting Information is available from the Wiley Online Library or from the author.

Conflict of Interest

The authors declare no conflict of interest.

[1] A. K. Geim, K. S. Novoselov, *Nat. Mater.* **2007**, *6*, 183.
[2] A. H. Castro Neto, F. Guinea, N. M. R. Peres, K. S. Novoselov, A. K. Geim, *Rev. Mod. Phys.* **2009**, *81*, 109.
[3] F. Bonaccorso, Z. Sun, T. Hasan, A. C. Ferrari, *Nat. Photonics* **2010**, *4*, 611.
[4] M. Z. Hasan, C. L. Kane, *Rev. Mod. Phys.* **2010**, *82*, 3045.
[5] X. L. Qi, S. C. Zhang, *Rev. Mod. Phys.* **2011**, *83*, 1057.
[6] H. J. Zhang, C. X. Liu, X. L. Qi, X. Dai, Z. Fang, S. C. Zhang, *Nat. Phys.* **2009**, *5*, 438.
[7] M. Chhowalla, H. S. Shin, G. Eda, L. J. Li, K. P. Loh, H. Zhang, *Nat. Chem.* **2013**, *5*, 263.
[8] B. Radisavljevic, A. Radenovic, J. Brivio, V. Giacometti, A. Kis, *Nat. Nanotechnol.* **2011**, *6*, 147.
[9] J. Wu, H. Schmidt, K. K. Amara, X. F. Xu, G. Eda, B. Ozyilmaz, *Nano Lett.* **2014**, *14*, 2730.
[10] M. Armand, J. M. Tarascon, *Nature* **2008**, *451*, 652.
[11] K. S. Kim, Y. Zhao, H. Jang, S. Y. Lee, J. M. Kim, K. S. Kim, J. H. Ahn, P. Kim, J. Y. Choi, B. H. Hong, *Nature* **2009**, *457*, 706.
[12] M. A. Py, R. R. Haering, *Can. J. Phys.* **1983**, *61*, 76.
[13] J. N. Coleman, M. Lotya, A. O'Neill, S. D. Bergin, P. J. King, U. Khan, K. Young, A. Gaucher, S. De, R. J. Smith, I. V. Shvets, S. K. Arora, G. Stanton, H. Y. Kim, K. Lee, G. T. Kim, G. S. Duesberg, T. Hallam, J. J. Boland, J. J. Wang, J. F. Donegan, J. C. Grunlan, G. Moriarty, A. Shmeliov, R. J. Nicholls, J. M. Perkins, E. M. Grieveson, K. Theuwissen, D. W. McComb, P. D. Nellist, V. Nicolosi, *Science* **2011**, *331*, 568.
[14] R. H. Friend, A. D. Yoffe, *Adv. Phys.* **1987**, *36*, 1.
[15] L. David, R. Bhandavat, G. Singh, *ACS Nano* **2014**, *8*, 1759.
[16] D. W. Murphy, F. A. Trumbore, *J. Cryst. Growth* **1977**, *39*, 185.
[17] L. A. Wray, S. Y. Xu, Y. Q. Xia, Y. S. Hor, D. Qian, A. V. Fedorov, H. Lin, A. Bansil, R. J. Cava, M. Z. Hasan, *Nat. Phys.* **2010**, *6*, 855.
[18] Y. S. Hor, J. G. Checkelsky, D. Qu, N. P. Ong, R. J. Cava, *J. Phys. Chem. Solids* **2011**, *72*, 572.
[19] Y. S. Hor, A. J. Williams, J. G. Checkelsky, P. Roushan, J. Seo, Q. Xu, H. W. Zandbergen, A. Yazdani, N. P. Ong, R. J. Cava, *Phys. Rev. Lett.* **2010**, *104*, 057001.
[20] J. X. Wu, H. T. Yuan, M. M. Meng, C. Chen, Y. Sun, Z. Y. Chen, W. H. Dang, C. W. Tan, Y. J. Liu, J. B. Yin, Y. B. Zhou, S. Y. Huang, H. Q. Xu, Y. Cui, H. Y. Hwang, Z. F. Liu, Y. L. Chen, B. H. Yan, H. L. Peng, *Nat. Nanotechnol.* **2017**, *12*, 530.

[21] Y. Liu, L. D. Zhao, Y. C. Liu, J. L. Lan, W. Xu, F. Li, B. P. Zhang, D. Berardan, N. Dragoe, Y. H. Lin, C. W. Nan, J. F. Li, H. M. Zhu, *J. Am. Chem. Soc.* **2011**, *133*, 20112.

[22] J. Li, J. H. Sui, Y. L. Pei, C. Barreteau, D. Berardan, N. Dragoe, W. Cai, J. Q. He, L. D. Zhao, *Energy Environ. Sci.* **2012**, *5*, 8543.

[23] G. Eda, H. Yamaguchi, D. Voiry, T. Fujita, M. W. Chen, M. Chhowalla, *Nano Lett.* **2011**, *11*, 5111.

[24] J. Yao, K. J. Koski, W. D. Luo, J. J. Cha, L. B. Hu, D. S. Kong, V. K. Narasimhan, K. F. Huo, Y. Cui, *Nat. Commun.* **2014**, *5*, 6670.

[25] W. Z. Bao, J. Y. Wan, X. G. Han, X. H. Cai, H. L. Zhu, D. H. Kim, D. K. Ma, Y. L. Xu, J. N. Munday, H. D. Drew, M. S. Fuhrer, L. B. Hu, *Nat. Commun.* **2014**, *5*, 4224.

[26] R. Kappera, D. Voiry, S. E. Yalcin, B. Branch, G. Gupta, A. D. Mohite, M. Chhowalla, *Nat. Mater.* **2014**, *13*, 1128.

[27] D. S. Hecht, L. B. Hu, G. Irvin, *Adv. Mater.* **2011**, *23*, 1482.

[28] B. A. Bernevig, T. L. Hughes, S. C. Zhang, *Science* **2006**, *314*, 1757.

[29] L. Fu, C. L. Kane, E. J. Mele, *Phys. Rev. Lett.* **2007**, *98*, 106803.

[30] X. L. Qi, T. L. Hughes, S. C. Zhang, *Phys. Rev. B* **2008**, *78*, 195424.

[31] X. A. Zhang, J. Wang, S. C. Zhang, *Phys. Rev. B* **2010**, *82*, 245107.

[32] H. L. Peng, W. H. Dang, J. Cao, Y. L. Chen, W. Wu, W. S. Zheng, H. Li, Z. X. Shen, Z. F. Liu, *Nat. Chem.* **2012**, *4*, 281.

[33] Y. F. Guo, M. Aisijiang, K. Zhang, W. Jiang, Y. L. Chen, W. S. Zheng, Z. H. Song, J. Cao, Z. F. Liu, H. L. Peng, *Adv. Mater.* **2013**, *25*, 5959.

[34] Y. F. Guo, L. Lin, S. L. Zhao, B. Deng, H. L. Chen, B. J. Ma, J. X. Wu, J. B. Yin, Z. F. Liu, H. L. Peng, *Adv. Mater.* **2015**, *27*, 4315.

[35] H. Li, J. Cao, W. S. Zheng, Y. L. Chen, D. Wu, W. H. Dang, K. Wang, H. L. Peng, Z. F. Liu, *J. Am. Chem. Soc.* **2012**, *134*, 6132.

[36] M. Lin, D. Wu, Y. Zhou, W. Huang, W. Jiang, W. S. Zheng, S. L. Zhao, C. H. Jin, Y. F. Guo, H. L. Peng, Z. F. Liu, *J. Am. Chem. Soc.* **2013**, *135*, 13274.

[37] K. J. Koski, J. J. Cha, B. W. Reed, C. D. Wessells, D. S. Kong, Y. Cui, *J. Am. Chem. Soc.* **2012**, *134*, 7584.

[38] K. J. Koski, C. D. Wessells, B. W. Reed, J. J. Cha, D. S. Kong, Y. Cui, *J. Am. Chem. Soc.* **2012**, *134*, 13773.

[39] K. P. Chen, F. R. Chung, M. J. Wang, K. J. Koski, *J. Am. Chem. Soc.* **2015**, *137*, 5431.

[40] W. H. Dang, H. L. Peng, H. Li, P. Wang, Z. F. Liu, *Nano Lett.* **2010**, *10*, 2870.

[41] F. Xiong, H. T. Wang, X. G. Liu, J. Sun, M. Brongersma, E. Pop, Y. Cui, *Nano Lett.* **2015**, *15*, 6777.

[42] Y. Y. Zhao, X. Luo, J. Zhang, J. X. Wu, X. X. Bai, M. X. Wang, J. F. Jia, H. L. Peng, Z. F. Liu, S. Y. Quek, Q. H. Xiong, *Phys. Rev. B* **2014**, *90*, 245428.

[43] J. Zhang, Z. P. Peng, A. Soni, Y. Y. Zhao, Y. Xiong, B. Peng, J. B. Wang, M. S. Dresselhaus, Q. H. Xiong, *Nano Lett.* **2011**, *11*, 2407.

[44] L. Y. Jiao, B. Fan, X. J. Xian, Z. Y. Wu, J. Zhang, Z. F. Liu, *J. Am. Chem. Soc.* **2008**, *130*, 12612.

[45] L. M. Zhang, J. W. Yu, M. M. Yang, Q. Xie, H. L. Peng, Z. F. Liu, *Nat. Commun.* **2013**, *4*, 1443.

[46] M. S. Dresselhaus, *Intercalation in Layered Materials, NATO ASI Series, Subseries B, Physics, Vol. 148*, Plenum Press, New York, **1987**.

[47] T. Jayasekera, B. D. Kong, K. W. Kim, M. B. Nardelli, *Phys. Rev. Lett.* **2010**, *104*, 146801.

[48] A. Sandin, T. Jayasekera, J. E. Rowe, K. W. Kim, M. B. Nardelli, D. B. Dougherty, *Phys. Rev. B* **2012**, *85*, 125410.

[49] H. Z. Geng, K. K. Kim, K. P. So, Y. S. Lee, Y. Chang, Y. H. Lee, *J. Am. Chem. Soc.* **2007**, *129*, 7758.

[50] V. Skakalova, A. B. Kaiser, U. Dettlaff-Weglikowska, K. Hrncarikova, S. Roth, *J. Phys. Chem. B* **2005**, *109*, 7174.

[51] T. Takenobu, T. Kanbara, N. Akima, T. Takahashi, M. Shiraishi, K. Tsukagoshi, H. Kataura, Y. Aoyagi, Y. Iwasa, *Adv. Mater.* **2005**, *17*, 2430.

1703424 (8 of 8)